PEER-REVIEWED ARTICLE

Parametric Modeling of Spaceborne SAR Image Geometry. Application: SEASAT/SPOT Image Registration

I. Tannous and B. Pikeroen

Abstract

A parametric modeling of the image geometry of spaceborne synthetic-aperture radar (SAR) sensor is presented. The model parameters are orbital parameters, sensor parameters and SAR processing parameters. This modeling allows geometric processing (points location, geocoding, registration), the accuracy of which is dependent only on parameter measurement errors. In addition, error models enable one to refine the parameters through Bayesian estimation by using control points (ground control points when a map is available, homologous points in the case of image registration). SEASAT/SPOT image registration is presented as an application. The relief effect is discussed and is decorrelated from the parameter error effect. The resulting pixel registration error is less than 10 metres if the relief effect is compensated for.

Introduction

For cartographic applications of remote sensing image and multi-sensor image interpretation (fusion), one needs to know accurately the geometric model (deformation model) between the images and a reference map (with or without a digital elevation model) and between the images themselves. Careful modeling of the spacecraft's physical properties enables one to express the deformation functions (or location functions) between the image geometry and the terrain geometry. To allow accurate geometric processing (points location, geocoding, image registration), these functions must have a parametric form. As a general rule, the physical properties of the image geometry are such that only a small number of parameters is sufficient to ensure sub-pixel accuracy. The interest of this approach is multiple:

- the parameters have a clear physical meaning, and their effects are easy to understand;
- the geometric image registration is then presented as the optimal estimation of parameters from observations;
- accuracy can be controled; and
- the modeling is often continuous and has slow variation. That allows its extrapolation to more than one scene.

In this paper, the image geometry of a spaceborne SAR sensor is discussed based on this parametric modeling approach.

The model parameters are part of the different segments of the imaging system; i.e.,

- spacecraft orbit,
- sensor (instruments), and
- SAR processing algorithm.

Before introducing the model parameters and errors affecting them in the section on parametric modeling, we will draw up, in the next section, the SAR sensor location function. In the final section, an application of the parametric modeling is presented. It is the registration of a SEASAT and a SPOT image of the Aix-en-Provence region (France).

SAR Location Function

The location function allows the computation of the coordinates of a point in any (arbitrary) geographic coordinate system from its image coordinates. This function is deduced from the raw data processing (SAR processing) that produces the image. SAR processing will not be described in detail in this paper, so for readers not familiar with this topic, see for example Barber (1985), Fitch (1988), and Wehner (1987).

SAR processing is separated into two parts corresponding to the two dimensions of the image:

- range processing followed by range migration correction, and
- azimuth processing.

In both directions, the processing consists of pulse compression achieved by a convolution of the return with a reference function $h(t) \alpha s^{\star}(-t)$ where $s(t)$ is the return in the considered direction ($\star$ denotes the complex conjugate) (Wehner, 1987). In the range direction, for a given target at slant range r from the sensor, the return is of the form (the amplitude of the signal is of no interest for geometric purpose)

$$s_r(t) \propto \exp\{2\pi\imath[f_{if}\, t + \frac{1}{2}\alpha(t-\tau)^2]\} \text{ with } -T/2 \le t-\tau \le T/2 \quad (1)$$

where we assume a transmitted chirp (linear frequency modulated signal) of carrier frequency f and rate $\alpha = \Delta f/T$ (Δf and T are, respectively, the bandwidth and the pulse duration). τ is the round trip delay time of the pulse and is equal to $2r/c$ with c the speed of light. f_{if} is the intermediate fre-

MATRA MS2i Signal and Image Processing Laboratory, 38 Boulevard Paul Cezanne, B.P. 235, 78052 Saint-Quentin-en-Yvelines Cedex, France.
Both authors are now with Thomson-CSF, 7, rue des Mathurins, 92223 Bagneux cedex, France.

Photogrammetric Engineering & Remote Sensing, Vol. 60, No. 6, June 1994, pp. 755–766.

0099-1112/94/6006–755$03.00/0

quency obtained after mixing down the received signal (the time t used in this direction is usually called the fast time because it is referenced to c).

In this direction the pulse compression is easily achieved because f_{if} and α are given in the sensor specifications. The image is then formed by taking the modulus of $s_r(t) * h(t)$ (*denotes the convolution operation). This is a *sinc* function $\left(\frac{\sin \pi x}{\pi x}\right)$, in which the main lobe position indicates the position of the pixel in the image. The main lobe occurs at $t = \tau = 2r/c$. That is, the position of an arbitrary pixel in the range direction is related to the slant range r from the sensor to the corresponding point on the ground. If the pixel position in the range direction is referenced by q, we can write

$$r = \mu q + r_0. \tag{2}$$

The scale factor μ is the pixel size in range direction and is equal to c/F_s, where F_s is the analog to digital sampling frequency (A/D SF) and r_0 is a constant (if $q = 0$ at the first sample of the range line, then r_0 must be the near slant range).

After the range migration correction step, the signal in the azimuth direction for a given target is of the form

$$s_a(t) \propto \exp\{-2\pi\imath[f_D(t - t_c) + \frac{1}{2}\dot{f}_D(t - t_c)^2]\} \quad \text{with } -\frac{T_a}{2} \le t - t_c \le \frac{T_a}{2} \tag{3}$$

(the time t in this direction is called the slow time by opposition to the fast time because it is referenced to the velocity of the spacecraft). In the Earth coordinate system $R_E = (O, \vec{e}_1, \vec{e}_2, \vec{e}_3,)$ (rotating with the Earth) centered at the Earth center O, assuming the spacecraft is denoted by S and the target by M (assumed fixed on the Earth surface), we have (Fitch, 1988)

$$f_D = -\frac{2}{\lambda r}(\vec{R}_M - \vec{R}_S) \bullet \vec{V}_S \tag{4}$$

$$\dot{f}_D = -\frac{2}{\lambda r}(|\vec{V}_S|^2 - (\vec{R}_M - \vec{R}_S) \bullet \vec{A}_S) \tag{5}$$

with

$\lambda = c/f$: carrier wavelength of the transmitted pulse,
T_a : duration of the synthetic aperture,
t_c : time corresponding to the center of the synthetic aperture,
$\vec{R}_M = \vec{OM} = (x,y,z)$: target position in R_E,
$\vec{R}_S = \vec{OS} = (X_S,Y_S,Z_S)$: spacecraft position in R_E,

$\vec{V}_S = \frac{d\vec{R}_S}{dt} = (VX_S, VY_S, VZ_S)$: spacecraft velocity in R_E, and

$\vec{A}_S = \frac{d\vec{V}_S}{dt} = (AX_S, AY_S, AZ_S)$: spacecraft acceleration in R_E.

The f_D term is commonly called the Doppler centroid because it physically corresponds to the signal frequency at the center of the synthetic aperture caused by the phase shift due to the radial velocity of the spacecraft. The $\dot{f}_D$ term is usually called the Doppler frequency rate. This is because $\dot{f}_D$ is approximately the first derivative of f_D.

The response in this direction has the same form as the response in the range direction. However, in order to achieve the compression, $h(t)$ must be computed by tracking the Doppler frequency history (f_D and $\dot{f}_D$) of the target (clutter lock and autofocusing techniques). As in the range direction, the result of the convulution's modulus is a *sinc* function. Assuming an error-free estimate of f_D and $\dot{f}_D$, its main lobe, which gives the pixel position in the azimuth direction, occurs at $t = t_c$.

The position of an arbitrary pixel in the azimuth direction is related to the time t for which the frequency of the azimuth response of the corresponding target is equal to the Doppler centroid f_D. If the pixel position in azimuth direction is referenced by p, we can write

$$t = kp + t_0 \tag{6}$$

The scale factor k is the pixel size in azimuth direction and is equal to N/F_r with N and F_r being, respectively, the number of look and the pulse repetition frequency (PRF). t_0 is a constant depending on the origine of p.

From the image coordinates (p, q) of a target, we get (t, r) from Equations 6 and 2. We can write in R_E:

$$r = ((\vec{R}_M - \vec{R}_S) \cdot (\vec{R}_M - \vec{R}_S))^{1/2} \tag{7}$$

$\vec{R}_M$ is the unknown and $\vec{R}_S$, given by the ephemeris data (see section on orbit parameters), is a function of t.

The knowledge of f_D, used in the reference function of the azimuth processing, gives a second relation between $\vec{R}_M$ and the pixel position (t, r):

$$f_D = -\frac{2}{\lambda r}(\vec{R}_M - \vec{R}_S) \cdot \vec{V}_S \tag{8}$$

$\vec{V}_S$ is given by the ephemeris data and is a function of t.

The pixel location on the ground is achieved (Curlander, 1982) by solving Equations 7 and 8 with the constraint stating that the target belongs to the Earth surface modeled by an ellipsoid as given by

$$\frac{x^2 + y^2}{(A_E + h)^2} + \frac{z^2}{(B_E + h)^2} = 1 \tag{9}$$

with A_E and B_E, respectively, the equatorial and the polar radius of the reference ellipsoid and h the elevation of the target above the reference ellipsoid.

Because the system formed by Equations 7, 8, and 9 is not linear, it is solved by an iterative numerical technique such as the Newton-Raphson technique.

Parametric Modeling

The location algorithm developed in the late section allows for automatic pixel location. The accuracy of this location is related to the accuracy of the

- ephemeris data (X_S, Y_S, Z_S, VX_S, VY_S, VZ_S),
- SAR data collection system (k, μ, r_0, t_0), and
- SAR processing algorithm (f_D).

The ephemeris data are not known accurately.

Instabilities arising in oscillators and other electrical components of the radar along with inhomogeneities in the atmosphere (Greene and Moller, 1962; Develet, 1964) cause a phase error in the signal in both range and azimuth directions. Another consequence of these instabilities are the deviation of the instruments from there ideal position so that the PRF, F_r, and the A/D SF, F_s, don't keep their nominal values. Finally, sampling window timing error and dating error cause errors in range and azimuth direction, respectively (error sources are listed by Howard (1987)).

Tests conducted with SEASAT SAR data by Curlander (1982) predict pixel location within 200 m. In order to improve the location accuracy, it is necessary to have a parametric modeling of the image geometry. This parametric modeling will allow estimates of the actual values of the parameters from observations (ground control points or homologous points). The estimate is achieved by the maximum-likelihood technique. The error models of the parameters then become necessary.

Errors in the ephemeris data are usually assumed to be normally distributed in a random process. The same assumption is usually made for the phase error (Greene, 1962; Develet, 1964). On a other hand, we know nothing about timing and dating errors and the form of errors affecting F_r and F_s. For simplicity of the computation, we will assume these errors are also normally distributed. The maximum-likelihood estimator then leads to the least-squares estimator.

Sensor and SAR Processor Parameters

The sensor and SAR processor parameters will be discussed following their effects in the range or azimuth directions.

Range direction

Considering phase error, the response in the range direction $s'_r(t)$ is, therefore, proportional to

$$\exp\{2\pi\iota[f_{if}t + \frac{1}{2}\alpha(t - \tau)^2] + \iota\Delta\phi(t)\} \tag{10}$$

where $\Delta\phi(t)$ is the uncompensated phase error. If we assume a quadratic form for this error, $\Delta\phi(t) = 2\pi(\Delta f_1 t + \frac{1}{2}\Delta f_2 t^2)$ (with $\Delta f_1 \ll f_{if}$ and $\Delta f_2 \ll \alpha$), the computation of $|s'_r(t) * h(t)|$ (*denotes the convolution operation and $|\cdot|$ the modulus) with $h(t) \propto s^*_r(-t)$ yields a *sinc* function whose main lobe occurs at $t = \tau + \Delta t$ where (see Appendix 1)

$$\Delta t = -\frac{\Delta f_1}{\alpha}. \tag{11}$$

This error corresponds to a slant range error $\Delta r = -\frac{c\Delta f_1}{2\alpha}$.

Sampling window timing error introduces an additional error Δr in this direction. Both errors can be compensated for by setting r_0 of Equation 2 as parameter in our model. Assuming these errors are constant for the whole scene, the parametrization of r_0 is: $r_0 = r_0^0$.

An error ΔF_s in the A/D SF is equivalent to an error $\Delta\mu = -\frac{c}{F_s^2}\Delta F_s$, causing a slant range error $\Delta r = \Delta\mu q$. If μ is considered to be a parameter, this error can be compensated for. We can assume this error constant for the whole scene yielding the parametrization of μ of the form $\mu = \mu_0$.

Azimuth Direction

In the azimuth direction, the form of the signal is given by Equation 3. The phase of the signal $\phi_D(u) = -2\pi(f_D u + \frac{1}{2}\dot{f}_D u^2)$ $(u = t - t_c)$ is the phase history of the target. But in practice the phase history recorded by the sensor differs from the actual phase history of the imaged target by an amount $\Delta\phi_D(u)$. This is caused by two sources: small changes in the radar carrier frequency or wavelength (causing a phase shift $\Delta\phi_{D_1}(u)$[1]) and instabilities in the receiver system (causing a phase shift $\Delta\phi_{D_2}(u)$[2]).

The global phase shift can be written as

$$\begin{aligned}\Delta\phi_D(u) &= \Delta\phi_{D_1}(u) + \Delta\phi_{D_2}(u) \\ &= -2\pi(\Delta f_D u + \frac{1}{2}\Delta\dot{f}_D u^2)\end{aligned} \tag{12}$$

so that the actual phase of the received azimuth signal $s'_a(u)$ is

$$\phi'_D(u) = -2\pi(f'_D u + \frac{1}{2}\dot{f}'_D u^2) \tag{13}$$

with $f'_D = f_D + \Delta f_D$ and $\dot{f}'_D = \dot{f}_D + \Delta\dot{f}_D$.

The azimuth reference function $h(u)$ is built by estimating the phase of the received signal $s'_a(u)$. Assuming error-free estimate, we have

$$h(u) = s'^*_a(-u) \propto \exp[2\pi\iota(-f'_D u + \frac{1}{2}\dot{f}'_D u^2)] \tag{14}$$

The image $|s'_a(u) * h(u)|$ is proportional to a *sinc* function in which the main lobe occurs at $u = 0$: i.e., $t = t_c$ (see Appendix 1).

The phase error occurring in the azimuth direction has no effect on the pixel position on the image grid (p, q). But it is clear that it will result a location error in azimuth direction by using f'_D in Equation 8 for localization.

This error can be removed by setting f_D as a parameter. In general, the parametrization of f_D is of the form

$$\begin{aligned}f_D &= f_{D0}(p) + f_{D1}(p)\, q + f_{D2}(p)\, q^2 \\ \text{with } f_{Di}(p) &= f_{Di0} + f_{Di1}\, p \;\; (i = 0,1,2)\end{aligned} \tag{15}$$

An error ΔFr on the PRF is equivalent to an error $\Delta k = -\frac{N}{F_r^2}\Delta Fr$, causing an error in the azimuth direction $\Delta t = \Delta k\, p$. If k is used as a parameter, this error can be compensated for. We can assume this error to be constant for the whole scene, yielding the parametrization of k of the form $k = k_0$.

Other errors occurring in the azimuth direction are timing errors:

- stop-start approximation gives an azimuth error $\Delta t = r/c$, and
- dating error (delay between command center and spacecraft operation).

This error can be removed by setting t_0 in Equation 6 as a parameter. This error is constant for the whole scene[3]. The parametrization of t_0 is then of the form $t_0 = t_0^0$.

---

[1] Another way to write the phase history is $\phi_D(u) = -\frac{4\pi}{\lambda}r(u)$. If the radar wavelength drifts to $\lambda' = \lambda + \Delta\lambda$, the corresponding phase shift is $\Delta\phi_{D_1}(u) = -\phi_D(u)\frac{\Delta\lambda}{\lambda}$.

[2] We know nothing about the value of this error.

[3] The stop-start approximation error is a function of the slant range r. For a SEASAT image, r varies approximately between 840 km and 880 km. With the azimuth pixel size $k \approx 2.410^{-3}$ s and $c \approx 310^8$ ms^{-1}, the corresponding error in azimuth direction varies between 1.16 and 1.22 pixels which can be considered as constant.

TABLE 1. RELATIVE INTENSITY OF GRAVITATIONAL FORCES.

Oblateness of the Earth (J2 term of the Earth gravitational potential)	10^{-03}
Irregularities of the Earth shape	10^{-05}
Moon attraction	10^{-07}
Sun attraction	10^{-07}
Sun pression	5.10^{-09}
Friction for a spacecraft (SPOT type)	10^{-09}

Note

The value of f_D used for localization in Equation 8 is the one estimated during azimuth processing to form the azimuth reference function. We will consider now an error on the estimate of the phase history of the target (f_D, $\dot{f}_D$).

Assume the estimated values are $\hat{f}_D = f_D + \Delta f_D$ and $\hat{\dot{f}}_D = \dot{f}_D + \Delta \dot{f}_D$ where f_D and $\dot{f}_D$ are the actual frequencies of the azimuth signal and, Δf_D and $\Delta \dot{f}_D$ are the estimate errors ($\Delta f_D \ll f_D$, $\Delta \dot{f}_D \ll \dot{f}_D$).

For the sake of simplifying the mathematics, we assume no error caused by the instruments. $h(u)$ ($u = t - t_c$) is then given by

$$h(u) \propto \exp\{2\pi\imath[-\hat{f}_D u + \frac{1}{2}\hat{\dot{f}}_D u^2]\}. \quad (16)$$

We can show (see Appendix 1) that the main lobe of $|s'_a(u) \star h(u)|$ occurs for $u \approx \frac{\Delta f_D}{\dot{f}_D}$. The pixel's position on the image is then

$$t \approx t_c + \frac{\Delta f_D}{\dot{f}_D} \quad (17)$$

(the effect of $\Delta \dot{f}_D$ on localization is negligible).

The result of an error Δf_D on the estimate of the Doppler centroid is a shift of the pixel in the azimuth direction by an amount $\Delta p = \Delta t/k$ with $\Delta t = \frac{\Delta f_D}{\dot{f}_D}$.

We show in Appendix 2 that, if $\hat{f}_D$ is used in Equation 8 for localization, the shift of the pixel in the image is compensated for naturally and the correct target is located on the ground: **error in the estimate of f_D during azimuth processing doesn't produce location error.**

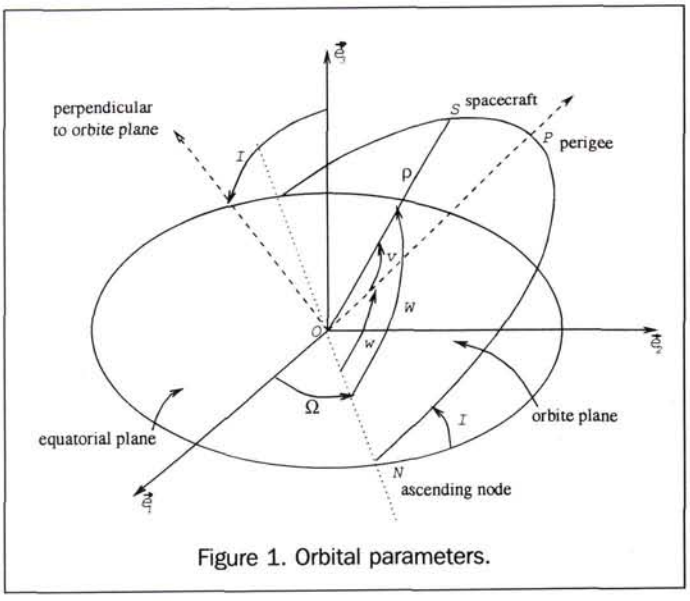

Figure 1. Orbital parameters.

Orbit Parameters

It is clear that the accuracy of the location is highly dependent on the accuracy of the ephemeris data. In a general rule, the ephemeris data are not known accurately and they must be refined. An accurate parametric orbit model is so necessary for high precision location or registration. It is the aim of this section.

Choice of a Model

The orbit of a spacecraft like SEASAT, ERS-1, or SPOT should satisfy the 0 order Kepler laws. It is an ellipse, where one focus is located at the Earth center, characterized by six known nominal parameters. In fact, different forces perturb the orbit, making it deviate from the nominal parameters. With respect to the gravitational force, the nature and the relative intensity of these forces are listed in decreasing order in Table 1 (CNES, 1980).

The gravitational force being the main force, it is possible to show that the spacecraft orbit is just slightly non-Keplerian. It is locally an ellipse. These ellipse parameters (called *osculatory* parameters) at a given time are those of the ellipse followed by the spacecraft if all the forces except the gravitational one were eliminated. These parameters are time dependent, but it is possible to show (Guichard, 1986) that **on a small orbit arc** (≈ 2000 km), **a Taylor series expansion of the osculatory parameters at a low order is enough to model the spacecraft motion with a very high accuracy**. The coefficients of these series expansion become the orbit model parameters. Such a modeling using the actual orbit parameters is more realistic and satisfactory than other parametric modeling like polynomial or spline. This modeling has further advantages:

- knowledge of the accuracy of the modeling: it is possible to compute analytically the neglected terms in the modeling and their effects on the ground versus the pertubatory terms of the Earth gravitational potential;
- some parameters are *a priori* known (without orbit measurements); the Lagrange equations allow one to rely on the higher order terms and the 0 order term;
- the number of parameters known with insufficient accuracy is for one scene very small (5 among 12);
- the physical nature and the rigidity of the modeling allow one to filter errors in the measurements of the ephemeris; and
- the unknown parameters can be estimated with a small number of ground control points.

For all these reasons, the choice of a modeling by the osculatory parameters is recommended. A more detailed mathematical analysis is described in the following sub-section.

Orbit Modeling Equations

Among the different orbit parametrizations, the more classical employs the following six parameters set (see Figure 1):

$$(a,e,I,w,n,\Omega)$$

(respectively, the semi-major axis, eccentricity, inclination,

perigree argument, true anomaly, and longitude of the ascending node). For an image, just a small arc of the orbit is of interest. In this case, it is more practical and more accurate to use the following set of parameters (see figure 1):

$$(\rho, I, W, \Omega, \eta_x, \eta_y)$$

(respectively, the distance from center of the Earth to the spacecraft, inclination, spacecraft argument, longitude of ascending node, $\eta_x = e\cos(W - w)$, and $\eta_y = e\sin(W - w)$). We can note that, among this set, the knowledge of the first four parameters are sufficient to define the spacecraft position.

The Lagrange equations allow one to know the time derivatives of the parameters versus the derivatives of the Earth gravitational potential perturbation function R with respect to the parameters. R can be expanded in Legendre polynomials whose main term R_{20} allows an accurate computation of the parameters for a few scenes (Guichard, 1986). All the derivatives of the osculatory parameters can be then expressed with respect to this term; this will allow one

- to know the order of the expansion of the parameters (depending on the wanted accuracy), and
- to establish the physical relationships between the parameters (this will allow one to constrain their variations for robustness, for example, false ground control points filtering).

We are then induced to build the following model (for small eccentricity orbits such as those for SEASAT, ERS-1, or SPOT):

$$\rho(t) = \rho_0 + \rho_1 t + \rho_2 t^2 + \rho_3 t^3 \quad (18)$$

$$I(t) = I_0 + I_1 t \quad (19)$$

$$W(t) = W_0 + W_1 t + W_2 t^2 + W_3 t^3 \quad (20)$$

$$\Omega(t) = \Omega_0 + \Omega_1 t \quad (21)$$

The ephemerides are related to these parameters in R_E by the following relationships:

$$X_S = \rho\,(\cos(W)\cos(\Omega) - \sin(W)\sin(\Omega)\cos(I)) \quad (22)$$

$$Y_S = \rho\,(\cos(W)\sin(\Omega) + \sin(W)\cos(\Omega)\cos(I)) \quad (23)$$

$$Z_S = \rho\sin(W)\sin(I) \quad (24)$$

$$VX_S = \frac{dX_S}{dt} \quad (25)$$

$$VY_S = \frac{dY_S}{dt} \quad (26)$$

$$VZ_S = \frac{dZ_S}{dt} \quad (27)$$

where the time derivative of the parameters are known versus the parameters themselves.

Inversely, the parameters are computed from the ephemeris data given at different time t_i by the following equations (developed in R_E):

$$\begin{aligned} c_x &= Y_S(t_i).VZ_S(t_i) - Z_S(t_i).VY_S(t_i) \\ c_y &= Z_S(t_i).VX_S(t_i) - X_S(t_i).VZ_S(t_i) \\ c_z &= X_S(t_i).VY_S(t_i) - Y_S(t_i).VX_S(t_i) \end{aligned}$$

$$c = \sqrt{c_x^2 + c_y^2 + c_z^2}$$

$$\rho(t_i) = \sqrt{X_S(t_i)^2 + Y_S(t_i)^2 + Z_S(t_i)^2} \quad (28)$$

$$I(t_i) = \arccos\frac{c_z}{c} \quad (29)$$

$$W(t_i) = \arcsin\frac{Z_S(t_i)}{\rho(t_i)\sin I(t_i)} \quad (30)$$

$$\Omega(t_i) = \arctan\frac{-c_x}{c_y} \quad (31)$$

The Taylor series expansion of these parameters is then deduced from these measurements by a least-squares technique.

Summary

The parametric location function can be represented by

$$(x,y,z) = \vec{G}_{SAR}(p,q,h;\vec{\theta}_{SAR}) \quad (32)$$

where

(x,y,z) are the coordinates of the target in R_E,

$\vec{G}_{SAR}$ is the SAR location function which doesn't have an analytical form,

$\vec{\theta}_{SAR} = (\theta_1, \ldots, \theta_n)$ is the parameters vector for the SAR image geometry.

Remark: during the least-squares process, the derivatives of (x,y,z) with respect to the parameters are needed. As $\vec{G}_{SAR}$ doesn't have an analytical form, the derivatives are computed by differentiating Equations 7, 8, and 9, yielding the solution of a linear system of three equations in (dx, dy, dz). $\frac{\partial\alpha}{\partial\theta_i}$ ($\alpha = x, y,$ or z and $i = 1, \ldots, n$) is then derived by computing $\frac{d\alpha}{d\theta_i}$ with $d\theta_j = 0$ for $j \neq i$. Finally, we can note that the relief effect is given by $\frac{\partial\vec{G}_{SAR}}{\partial h}$.

Application: SEASAT/SPOT Image Registration

As application of this parametric modeling, we present the registration of a SEASAT SAR image (revolution no. 719, digitally correlated by the Jet Propulsion Laboratory) with a panchromatic SPOT image (©SPOT image 1986, CNES) on the Aix-en-Provence (France) region, according a new approach.

The registration problem comes to a parametric estimation problem. The specific problem posed by relief is taken into account. We will first speak about the parametric estimation process, which is in fact an optimization process, giving some accuracy estimates of the registration, and then we will present some registration examples.

Parametric Estimation Process

Initialization

To begin the estimation process, the parameters $\vec{\theta}_{SAR}$ must be initialized to an *a priori* value $\vec{\theta}^{\,0}_{SAR}$.

A set of 20 ephemeris data sampled every second was available with the SAR image. They first have been expressed in R_E. $(\rho(t_i), I(t_i), W(t_i), \Omega(t_i))$ for $i = 1,\ldots,20$ are then computed using Equations 28 to 31. The initial values of the orbit parameters $(\rho_0, \rho_1, \rho_2, \rho_3, I_0, I_1, W_0, W_1, W_2, W_3, \Omega_0, \Omega_1)$ are finally derived by a least-squares technique.

In practice, among these parameters, just the values of (ρ_0, ρ_1, W_0, W_1, Ω_0) must be refined by estimation from observations. In general, the accuracy of the other parameters is sufficient to preserve their initial values (Tannous, 1991).

With F_r = 1646.7 Hz, F_s = 45.53 MHz, N = 4, and c = 2.997925×10^8 ms^{-1}, we get the initial values for the parameters μ_0 and k_0:

$$\mu_0 = 6.58 \text{ m and } k_0 = 2.43 \times 10^{-3} \text{ s}$$

The value of k_0 is not refined because errors affecting this parameter can be compensated for by the orbit parameters.

The initial values of r_0^0 and t_0^0 are taken as the slant range to near edge of the image and the image center time, respectively, both given in the auxillary data:

r_0^0 = 844.11 km
t_0^0 = 06 h 38 min 06 sec of 16 August 1978

$q = 0$ is then the first azimuth line and $p = 0$ is the center range line. The value of t_0^0 is not refined because errors affecting this parameter can be compensated for by the orbit parameters.

The Doppler centroid used in the azimuth reference function is:

$$f_D = A\,q^2 + B\,q + C$$

with $A = 0$, $B = -68.54 \times 10^{-3}$ Hz, and $C = -713.46$ Hz. That gives the initial values of the Doppler parameters:

$$f_{D00} = C \text{ and } f_{D10} = B$$

all other parameters f_{Dij} being zero.

We take the parametrization of f_D in the same way as used in azimuth processing. Then, only the values of f_{D00} and f_{D10} are refined to compensate for the errors due to phase shift of the received signal in azimuth direction; the other parameters keep their initial values.

The total number of parameters to be refined by estimation from observations for the SAR image is then n = 9.

Optimization

A parametric modeling of SPOT image geometry has been developed by Pikeroen (Pikeroen, 1991). The derived SPOT location function is represented by

$$(x,y,z) = \vec{G}_{SPOT}\,(p,q,h;\,\vec{\theta}_{SPOT}) \qquad (33)$$

where $\vec{\theta}_{SPOT}$ is the vector of parameters of the SPOT parametric model.

A set of values H_i for only N_H = 14 homologous pixels ($H_i = (p_{1i}, q_{1i}; p_{2i}, q_{2i})$, subscript 1 is set for the SEASAT image while subscript 2 is set for the SPOT image, and $i = 1,\ldots,N_H$) has been taken between the two images. They are chosen uniformly distributed over the 5376- by 5760-pixel SEASAT image and the 6000- by 6000-pixel SPOT image.

If we define the residual of localization for the i^{th} homologous pixels as

$$\vec{F}_i\,(\vec{\theta}_{SPOT}, \vec{\theta}_{SAR}) = \vec{G}_{SPOT}\,(p_{2i}, q_{2i}, h_i; \vec{\theta}_{SPOT}) - \vec{G}_{SAR}\,(p_{1i}, q_{1i}, h_i; \vec{\theta}_{SAR})$$

(if the models parameters were perfectly known, $\vec{F}_i$ would be zero) and if $\vec{\theta}^0_{SPOT}$ is the initial vector of parameters of the SPOT model, the Bayesian formulation leads to minimize

$$J(\vec{\theta}_{SAR}, \vec{\theta}_{SPOT}) = J_{obs}\,(\vec{\theta}_{SAR}, \vec{\theta}_{SPOT}) + J_0\,(\vec{\theta}_{SAR}, \vec{\theta}_{SPOT})$$

where

$$J_{obs}(\vec{\theta}_{SAR}, \vec{\theta}_{SPOT}) = \sum_{i=1}^{NH} \vec{F}_i^T(\vec{\theta}_{SAR}, \vec{\theta}_{SPOT})\,\Gamma^{-1}_{obs_i}\,\vec{F}_i\,(\vec{\theta}_{SAR}, \vec{\theta}_{SPOT})$$

where Γ_{obs_i} is a covariance matrix deduced from the observation error models (assumed Gaussian),

$$J_0(\vec{\theta}_{SAR}, \vec{\theta}_{SPOT}) = (\vec{\theta}_{SAR}, \vec{\theta}^0_{SAR})^T\,\Lambda^{-1}_{SAR}\,(\vec{\theta}_{SAR} - \vec{\theta}^0_{SAR}) + (\vec{\theta}_{SPOT} - \vec{\theta}^0_{SPOT})^T\,\Lambda^{-1}_{SPOT}\,(\vec{\theta}_{SPOT} - \vec{\theta}^0_{SPOT}) \text{ with}$$

Λ_{SAR} = E ($\vec{\epsilon}^T_{SAR}\,\vec{\epsilon}_{SAR}$) is the initial covariance matrix on $\vec{\theta}_{SAR}$, with $\vec{\epsilon}_{SAR} = \vec{\theta}_{SAR} - \vec{\theta}^0_{SAR}$,

Λ_{SPOT} = E ($\vec{\epsilon}^T_{SPOT}\,\vec{\epsilon}_{SPOT}$) is the initial covariance matrix on $\vec{\theta}_{SPOT}$, with $\vec{\epsilon}_{SPOT} = \vec{\theta}_{SPOT} - \vec{\theta}^0_{SPOT}$,

the T symbol and E(x) denote the transposition operation and the expected value of x, respectively.

$\vec{\epsilon}_{SAR}$ and $\vec{\epsilon}_{SPOT}$ are set to constrain the variation of the parameters within an interval centered on $\vec{\theta}^0$. The variation of the parameters are controlled by the standard deviation, $\sigma_{\vec{\theta}}$, of the gaussian assumed error models. $\sigma_{\vec{\theta}}$ must be derived from the sensor specifications (as we don't have the exact SEASAT sensor specifications about error models, the value of $\sigma_{\vec{\theta}}$ has been chosen arbitrarily, keeping in mind the physical meaning of the parameters).

That leads to a non-linear least-squares problem which can be shown to be locally convex. The initial value of ($\vec{\theta}_{SAR}$, $\vec{\theta}_{SPOT}$) is good enough to let the optimization converge to the right minimum of the problem. The problem can be solved by any suitable technique (quasi Newton, Gauss-Newton, conjugate gradient, ...).

The refined value of the parameters defines then the **relative distortion model** between the two images.

Note

In the optimization process, we assume implicitely that the elevation of h_i of the homologous points was known, which, in fact, is not the case. So, to allow a correct optimization process, h_i must be computed for each homologous point. The relief computation is presented in the next section.

Relief Computation and Accuracy of the Registration

Let us define an arbitrary cartographic coordinate system R_{carto} = (x, y, z), where the x and y axes define the East and North directions, respectively, while the z axis represents the elevation. The $z = 0$ plane is an arbitrary reference plane (for example, corresponding to the elevation h_0 above the ellipsoide). We know the transformation to go from R_E to R_{carto}, so that we can write the SAR and the SPOT location function in R_{carto} as

$$(x, y) = \vec{G}_{SAR}(p,q,z = h;\vec{\theta}_{SAR})$$

$$(x, y) = \vec{G}_{SPOT}(p,q,z = h;\vec{\theta}_{SPOT})$$

(in order to simplify, we have kept the same notation used in Equations 32 and 33).

The relative relief effect between the SAR and the SPOT image in the (x, y) plane for the i^{th} point is then given by the vector

$$\vec{\epsilon}_i(z) = \frac{\partial \vec{G}^{-1}_{SPOT}}{\partial z} - \frac{\partial \vec{G}^{-1}_{SAR}}{\partial z} \equiv \frac{\partial \vec{F}_i}{\partial z} = (\epsilon_{ix}(z), \epsilon_{iy}(z)).$$

The direction defined by $\vec{\epsilon}_i(z)$ is the **epipolar** direction, provided the epipolar curves exist (Guichard, 1986). The existence of the epipolar curves for a SPOT image and a SAR image, and the interval in which they can be considered as straight lines, have been proved in Tannous (1991).

If the (x, y, z) axis system is rotated by an angle $\chi = \arctan\left(\frac{\epsilon_{iy}(z=0)}{\epsilon_{ix}(z=0)}\right)$ around the z axis to get the new (u, v, z) coordinate system, then the u-component of the residual $F_{iu}(z = 0)$ is due only to the relief error while the v-component of the residual $F_{iv}(z = 0)$ is caused by errors on the parameters. That allows the computation of the elevation of the targets corresponding to the homologous points.

Given the elevation h_i of the i^{th} target, then $F_{iu}(z = h_i) = 0$. Expanding $F_{iu}(z = h_i)$ in a Taylor series about $z = 0$ and neglecting terms of order higher than 1 (Tannous, 1991) gives the elevation h_i of the target:

$$h_i = -\frac{F_{iu}(z=0)}{\epsilon_{iu}(z=0)} \equiv -\frac{F_{iu}(z=0)}{\sqrt{\epsilon_{ix}(z=0)^2 + \epsilon_{iy}(z=0)^2}}$$

where $\epsilon_{iu}(z = 0)$ is the u-component of $\vec{\epsilon}_i(z = 0)$ (its v-component is 0). In general, if we assume elevation h_i for a target, the error Δh_i on h_i is given by

$$\Delta h_i = -\frac{F_{iu}(z=h_i)}{\sqrt{\epsilon_{ix}(z=h_i)^2 + \epsilon_{iy}(z=h_i)^2}}. \quad (34)$$

We can now describe the optimization scheme along with the computation of the elevation.

Suscript 1 is set for SAR image and Subscript 2 is set for the SPOT image:

(1) *Initialization:* $\vec{\theta}_{1new} = \vec{\theta}^0_1$, $\vec{\theta}_{2new} = \vec{\theta}^0_2$ and $h_i = 0$ $(i = 1, ..., N_H)$
(2) *Optimization* with $\vec{\theta}_1 = \vec{\theta}_{1new}$, $\vec{\theta}_2 = \vec{\theta}_{2new}$ and $z = h_i$ $(i = 1,..., N_H)$
(3) *Result:* $\vec{\theta}_{1new}, \vec{\theta}_{2new}, \vec{F}_i(z = h_i), \vec{\epsilon}(z = h_i)$ $(i = 1, ..., N_H)$
(4) *Computation of* h_i: $h_i = h_i + \Delta h_i$ (Δh_i is given by Equation 34 and $i = 1, ..., N_H$)
(5) *go to (2):* because the model parameters and the elevation are in fact correlated, we need to iterate the process to converge to the actual elevation (three iterations are sufficient).

The RMS error on $F_{iv}(z = h_i)$ (for $i = 1, ..., N_H$), which represents the final error caused by the residual errors on the parameters, has been computed. We get

$$\text{RMS} = 8.684 \text{ metres.}$$

This result has been controlled by comparing the residuals of some other homologous points with known elevation (control points). All the residuals were less than 10 metres. Those results are better than the resolution of both images (10 metres for SPOT and about 25 metres for SEASAT)!

Illustration of the Registration

Using the estimated parameters, any pixel in one of the images can now be located in the other image using equations

$$(p_{2i}, q_{2i}) = \vec{G}^{-1}_{SPOT} \circ \vec{G}_{SAR}(p_{1i}, q_{1i}, h_i) \quad (35)$$

$$(p_{1i}, q_{1i}) = \vec{G}^{-1}_{SAR} \circ \vec{G}_{SPOT}(p_{2i}, q_{2i}, h_i) \quad (36)$$

where $\vec{G}^{-1}$ denotes the inverse function of $\vec{G}$, and $\circ$ the composition operation.

The elevation h_i of the pixel must be known to get accurate registration. This elevation can be got from a digital elevation model (DEM) or computed in the same way described in the previous section. This is illustrated on Plate 1. A curve has been drawn on the SPOT image (representing a river) and projected on the SEASAT image using our model (Equation 36). When the pixels elevation is not known (h_i is set to zero), we get the red curve on the SEASAT image, while the knowledge of this elevation gives very accurate location (green curve).

An application of that accurate geometric conformity between the SAR image and the SPOT image can be fusion of both data. For example, on Plate 2, a runway seen on the SPOT image has been drawn and projected on the SEASAT image using Equation 36 with known elevation. On Plate 3, a set of bright points (corresponding to electricity pylons) seen on the SEASAT image has been drawn and projected on the SPOT image using Equation 35 with known elevation. Finally, Plate 4 shows a region of the SPOT image resampled in the SEASAT image geometry, using Equation 35 with known elevation, and superimposed.

Notes

(1) If the SPOT image is replaced by a map (or a DEM), our parametric modeling along with a few ground control points allows one to achieve a highly accurate rectified image (or geocoded image) in the same way described in this paper.
(2) If the SPOT image is replaced by a SAR image, the optimized relative model can be used along with a correlation process to derive the DEM of the scene from the images (stereo). The homologous pixels are found by correlation along the epipolar direction defined in this section (the existence of the epipolar curves for two SAR images and the interval in which they can be considered as linear have been proved in Tannous 1991). This gives the residuals F_u (called parallax). The elevation of each pixel is then computed in the way described in the last section.

Conclusions

In this paper, we have presented a new parametric modeling of spaceborne SAR image geometry. The model parameters are

- orbital parameters,
- sensor parameters, and
- SAR processing parameters.

The elevation of the targets is considered in the modeling. The SAR location function, which allows the computation of the geographic coordinates of a target from its image coordinates and its elevation, is then deduced. The accuracy of the location function depends on the accuracy of the model parameters. The parametric characteristic of the modeling allows one to improve the accuracy of further geometric processings (points location, geocoding, DEM ex-

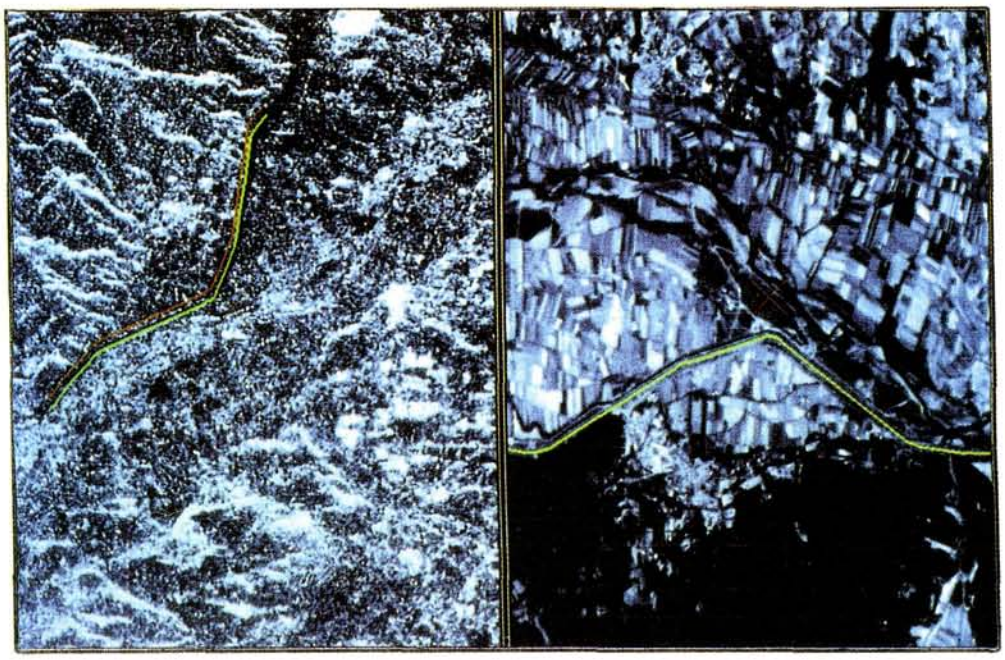

Plate 1. Illustration of relief effect in registration. A river drawn on the SPOT image (right image) has been projected on the SEASAT image (left image), with unknown elevation (red curve) and known elevation (green curve).

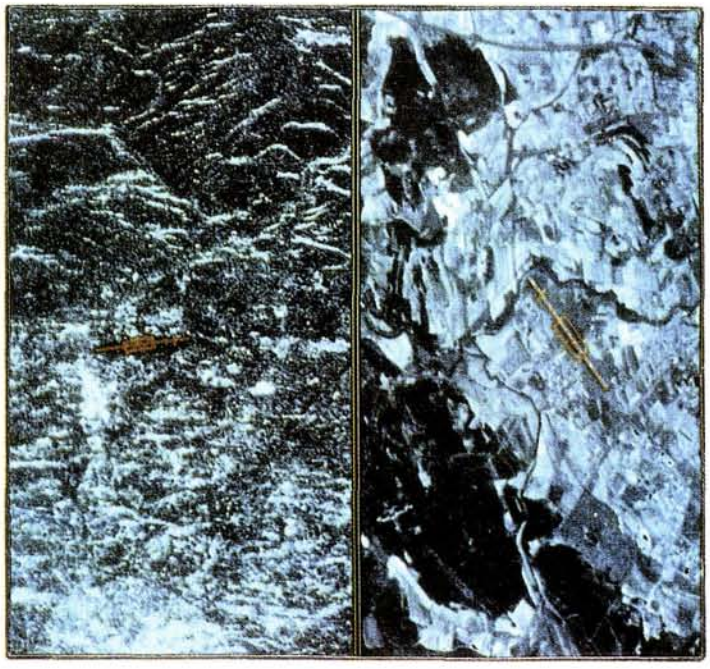

Plate 2. Projection of a runway on the SEASAT image.

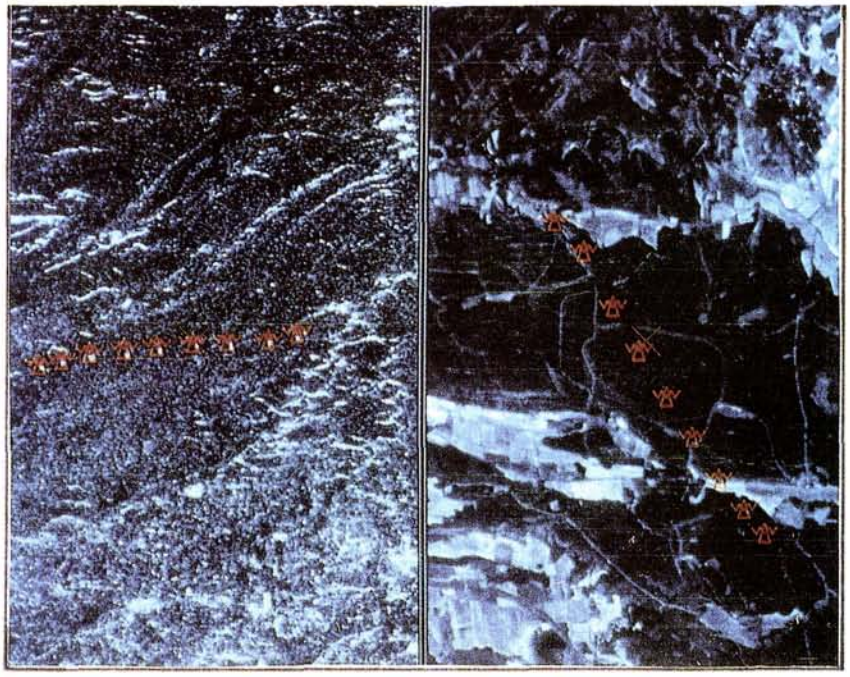

Plate 3. Projection of a set of electricity pylons on the SPOT image.

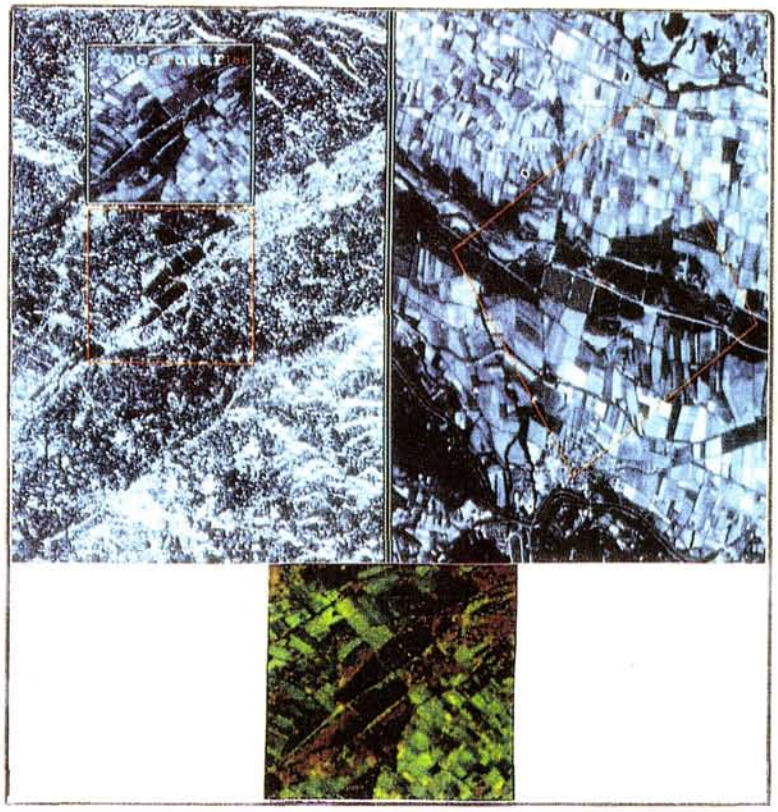

Plate 4. A region of the SPOT image resampled and superimposed on the SEASAT image.

traction by stereo, image registration) by use of the observations

- ground control points for geocoding (absolute location), and
- homologous points for registration (relative location).

The problem can be seen as an optimization problem in which the model parameters are estimated from the observations. The least-squares estimation technique is used. Registration of a SEASAT SAR image and a SPOT image is presented as an application. The accuracy achieved is sub-pixel.

The approach to the problem of geometric processings presented in this paper may become the basis of easily evolutionary multi-sensor systems. To deal with a new sensor, one only has to develop its parametric location function $\vec{G}$. The optimization process and all the geometric processings (points location, geocoding, DEM extraction, registration), which handle the generic functions $\vec{G}$, remain unchanged.

Remarks

- The optimization process presented in this paper takes into account observations which are only points (homologous points and ground control points). To arrive at fully automatic geometric processings, the optimization process must be able to deal with other kinds of observations such homologous linear features (obtained by image segmentation followed by matching process).
- Errors in the ephemeris have the most important effect on location. So with future systems with very accurate ephemeris measurements, such as Global Positioning System, SAR will become a very highly accurate target location system.

References

Barber, B. C., 1985. Theory of Digital Imaging from Orbital Synthetic-Aperture Radar, *Int. J. Remote Sensing*, 6(7):1109–1057.

CNES, 1980. *Mouvement du véhicule spatial en orbite*, report.

Curlander, J. C., 1982. Location of Spaceborne SAR Imagery, *IEEE Trans. on Geosc. and Rem. Sens.*, GE-20 (3): 359–364.

Develet, J. A., Jr., 1964. The Influence of Random Phase Errors on the Angular Resolution of Synthetic Aperture Radar Systems, *IEEE Trans. on Aerospace and Navigational Electronics*, ANE-11 (1): 58–67.

Fitch, J. P., 1988. *Synthetic Aperture Radar*, Springer-Verlag, 170 p.

Greene, C. A., and R. T. Moller, 1962. The Effect of Normally Distributed Random Phase Errors on Synthetic Array Gain Pattern, *IRE Trans. on Military Electronics*, Vol. MIL-6, No. 2, pp. 130–139.

Guichard, H., 1986. *Géométrie des Images de Satellite à défilement et application à la Photogrammétrie spatiale*, SPOT Image report.

Howard, P. D., 1987. The Impact of SAR Processing Algorithms on Geocoding of SAR Imagery, *Proceedings, Workshop on Image Rectification Techniques for Spaceborne SAR*, 14–16 January, Loipersdorf, Austria, pp. 51–55.

Pikeroen, B., 1991. *Modélisation géométrique multicapteurs: application à la stéréo et à la superposition d'images*, Rapport interne - MATRA LTIS.

Tannous, I., 1991. *Modélisation paramétrique de la géométrie de prise de vue du radar à ouverture synthétique embarqué sur satellite. Application à la superposition d'images radar/optique*, PhD thesis, Université PARIS VII.

Wehner, D. R., 1987. *High Resolution Radar*, Artech House, Norwood, Massachusetts, 472 p.

(Received 16 September 1991; revised and accepted 21 October 1992)

Appendix 1
Phase Mismatch Effect on Location

The received signals in range and azimuth direction are, respectively,

$$s_r(u) \propto \exp\left[2\pi\imath\left(f'_1 u + \frac{1}{2} f'_2 u^2\right)\right]$$

$$s_a(u) \propto \exp\left[-2\pi\imath\left(f'_1 u + \frac{1}{2} f'_2 u^2\right)\right]$$

with $f'_1 = f_1 + \Delta f_1$ and $f'_2 = f_2 + \Delta f_2$, where Δf_1 and Δf_2 are the errors induced by the phase shift.

range direction

$f_1 = f_{if}$,
$f_2 = \alpha$,
$u = t - \tau$ where τ is the round trip delay, and
by setting $u = 0$ at the middle of the pulse, we have

$$-\frac{T}{2} \le u \le \frac{T}{2}.$$

azimuth direction

$f_1 = f_D$,

$f_2 = \dot{f}_D$,

$u = t - t_c$ where t_c is the time corresponding to the center of the synthetic aperture, and

by setting $u = 0$ at the center of the synthetic aperture, we have $-\frac{T_a}{2} \le u \le \frac{T_a}{2}$.

The processing consists of convolving the signal with the reference function $h(u) \propto \hat{s}^*(-u)$ where $\hat{s}$ is the estimate of s (* denotes the complex conjugate):

range direction, $h(u)$ is build from the theoretically transmitted signal:

$$h_r(u) \propto \exp\left[-2\pi\imath\left(-f_1 u + \frac{1}{2} f_2 u^2\right)\right]$$

azimuth direction, $h(u)$ is build from the received signal by estimating its frequencies: i.e.,

$$h_a(u) \propto \exp\left[2\pi\imath\left(-f''_1 u + \frac{1}{2} f''_2 u^2\right)\right]$$

with $f''_1 = f'_1 + \Delta f'_1$ and $f''_2 = f'_2 + \Delta f'_2$ where $\Delta f'_1$ and $\Delta f'_2$ are estimation errors.

After processing, the signal is $s'(u) = s(u) * h(u)$. The image $I(u)$ is then formed by taking the modulus of $s'(u)$.

Range Direction

$$I(u) = |s'_r(u)| = \left| \int_{-T/2}^{+T/2} s_r(v) h_r(u - v)\, dv \right|$$

$$\Leftrightarrow I(u) \propto \left| \int_{-T/2}^{+T/2} \exp\left[2\pi\imath\left(\Delta f_1 v + f_2 uv + \frac{1}{2}\Delta f_2 v^2\right)\right] dv \right|$$

I(u) can be written as

$$I(u) \propto \left| \int_{-T/2}^{+T/2} \exp\{2\pi\iota[\frac{\Delta f_2}{2}(v + \frac{\Delta f_1 + f_2 u}{\Delta f_2})^2]\}dv \right|$$

$$= \left|\frac{1}{\alpha}\int_{\alpha(\frac{T}{2}+\omega)}^{\alpha(\frac{T}{2}+\omega)} \{\cos(\frac{\pi}{2}x^2) + \frac{\Delta f_2}{|\Delta f_2|}\,\iota\,\sin(\frac{\pi}{2}x^2)\}dx\right|$$

where it holds $x = \alpha(v + \omega)$, with $\alpha = \sqrt{2|\Delta f_2|}$ and $\omega = \frac{\Delta f_1 + f_2 u}{\Delta f_2}$. $I(u)$ can be written in terms of Fresnel sine and cosine integrals: i.e.,

$$C(y) = \int_0^y \cos(\frac{\pi}{2}x^2)dx$$

$$S(y) = \int_0^y \sin(\frac{\pi}{2}x^2)dx$$

hence

$$I(u) \propto \left|\frac{1}{\alpha}[C(\alpha(\frac{T}{2}+\omega)) + C(\alpha(\frac{T}{2}-\omega))] + \frac{1}{\alpha}\frac{\Delta f_2}{|\Delta f_2|}\iota[S(\alpha(\frac{T}{2}+\omega)) + S(\alpha(\frac{T}{2}-\omega))]\right|. \quad (37)$$

By solving $\frac{dI(u)}{du} = 0$, the maxima of $I(u)$ are found for $\omega = \frac{2n}{\alpha^2 T}$ where n is an integer.

The main lobe, which indicates the pixel position in the image, occurs for $n = 0$, i.e., by replacing ω by its value

$$u = t - \tau = -\frac{\Delta f_1}{f_2}.$$

This means that a target at a distance r from the sensor is imaged on the azimuth line corresponding the distance r' such that

$$r' = r - \frac{c}{2}\frac{\Delta f_1}{f_2}.$$

This shift of the pixel in the image will induce a location error of the target. This error can be compensated for by the parametric estimation. We can note that error on the rate of the received signal (Δf_2) has no effect on localization.

Azimuth Direction

To show the effect of Δf_1 and Δf_2, we assume first that $\Delta f_1' = 0$ and $\Delta f_2' = 0$ (error-free estimation).

We have then

$$I(u) \propto \left|\int_{-Ta/2}^{Ta/2} \exp[-2\pi\iota f_2'\ uv)]dv\right|$$

$$= |T_a \frac{\sin(\pi f_2' u\ T_a)}{\pi f_2' u T_a}|.$$

$I(u)$ is maximum for $u = 0$. The pixel is on the range line corresponding to $t = t_c$, i.e., the errors on the phase of the received signal don't affect the pixel position on the image grid. But use of f_1' to locate the target on the ground will introduce a location error which will be compensated for by the parametric estimation.

In the general case, if $\Delta f_1' \neq 0$ and $\Delta f_2' \neq 0$, we have

$$I(u) \propto \left|\int_{-Ta/2}^{Ta/2} \exp\{-2\pi\iota\,(\Delta f_1' v + \frac{1}{2}\Delta f_2'\ v^2 - f_2''\,u\ v)\}\ dv\right|$$
$$= \left|\int_{-Ta/2}^{Ta/2} \exp\{-2\pi\iota\,[\frac{\Delta f_2'}{2}(v + \frac{\Delta f_1' - f_2''\,u}{\Delta f_2'})^2]\}dv\right|.$$

The same calculation as in the range direction case yields the same result for $I(u)$ (Equation 37) with $\alpha = \sqrt{2|\Delta f_2'|}$ and $\omega = \frac{\Delta f_1' - f_2''\,u}{\Delta f_2'}$. The main lobe of $I(u)$ occurs for $\omega = 0$, i.e., for

$$u = t - t_c = \frac{\Delta f_1'}{f_2''}.$$

Because $(\Delta f_2 + \Delta f_2') \ll f_2$, we can make the following approximation:

$$u \approx \frac{\Delta f_1'}{f_2}.$$

The estimation error $\Delta f_1'$ will shift the pixel on the image grid so that its position will be on the range line corresponding to the time

$$t = t_c + \frac{\Delta f_1'}{f_2}.$$

We show in Appendix 2 that this shift in the image doesn't affect the location of the target if f_1'' is used in the location function (without taking into acount the errors due to the signal phase shift).

Appendix 2
Effect of Estimated Doppler Centroid on Location

The actual Doppler centroid of a target M is in R_E:

$$f_D = -\frac{2}{\lambda r}\vec{R}\ (t) \cdot \vec{V}_S(t) \quad (38)$$

with

λ = radar wavelength,
t = the time corresponding to the center of the synthetic aperture,

$\vec{R}\ (t) = \vec{SM}(t)$ where S denotes the spacecraft,

$\vec{V}\ (t) = \frac{d\vec{R}}{dt}$, and

$r = |\vec{R}\ (t)|$.

We assume no errors introduced by the instruments and atmospheric refraction. In the ideal case where f_D is estimated without any error during azimuth processing, the pixel position on the image grid is the range line corresponding to time t and, Equation 38 allows location of the target M from its position in the image.

In practice, we have an estimation error in f_D. The estimate of f_D is then

$$\hat{f}_D = f_D + \Delta f_D. \quad (39)$$

We show in Appendix 1 that the pixel position on the

image grid is then the range line corresponding to time $t' = t + \Delta t$ where

$$\Delta t = \frac{\Delta f_D}{\dot{f}_D} \tag{40}$$

with

$$\dot{f}_D \approx \frac{2}{\lambda r}(|\vec{V}_S(t)|^2 - \vec{R}(t) \cdot \vec{A}_S(t)).$$

We will show that use of $\hat{f}_D$ in Equation 38 allows location of the target (the knowledge of Δf_D is not useful).

Assume that the target satisfies the condition

$$\hat{f}_D = -\frac{2}{\lambda r}\vec{R}(t') \cdot \vec{V}_S(t'), \tag{41}$$

Then, expanding $\vec{R}$ and $\vec{V}_S$ in a Taylor series about t yields

$$\vec{R}(t') = \vec{R}(t) - \Delta t\, \vec{V}_S(t) - \frac{1}{2}\Delta t^2 \vec{A}_S(t) \tag{42}$$

$$\vec{V}_S(t') = \vec{V}_S(t) + \Delta t\, \vec{A}_S(t) \tag{43}$$

while $\frac{d\vec{A}_S}{dt}$ is neglected for orbiting sensors. Equation (41) becomes

$$\hat{f}_D = \frac{2}{\lambda r}(-\vec{R}(t) \cdot \vec{V}_S(t) + \Delta t\,(|\vec{V}_S(t)|^2 - \vec{R}(t) \cdot \vec{A}_S(t)) + \Delta t^2(\frac{3}{2}\vec{V}_S(t) \cdot \vec{A}_S(t)) + \Delta t^3(\frac{|\vec{A}_S(t)|^2}{2})). \tag{44}$$

In the case of orbiting sensors $\vec{V}_S \cdot \vec{A}_S$ and $|\vec{A}_S(t)|^2$ are negligible. With Equations 38 and 39, Equation 44 gives

$$\Delta f_D = \frac{2}{\lambda r}[|\vec{V}_S(t)|^2 - \vec{R}(t) \cdot \vec{A}_S(t)]\Delta t \Leftrightarrow \Delta t = \frac{\Delta f_D}{\dot{f}_D}$$

$(\hat{f}_D, t', r)$ satisfies Equation 38 only if $\Delta t = \frac{\Delta f_D}{\dot{f}_D}$, which is actually the shift of the pixel in the image grid.

So the estimation error Δf_D has no effect on location of the target.